J Nanostruct 12(3): 999-1012, Summer 2022

RESEARCH PAPER

Effects of Different Biosynthesis Methods on the Structural and Optical Properties of Iron Oxide Nanoparticles and Photocatalytic Application

Husam A. Khamees and Muslim A. Abid

Department of physics, College of Science, Mustansiriyah University, Baghdad, Iraq

ARTICLE INFO

Article History:
Received 21 July 2022
Accepted 27 September 2022
Published 01 October 2022

Keywords:
MB dye
Conocarpus Extract
IONPs
Photocatalytic Activity
Sol-gel Method

ABSTRACT

A simple chemical technique and the sol-gel method were used to manufacture iron oxide nanoparticles (IONPs). Conocarpus extract converts iron salts into IONPs. The process changes iron oxide NPs from $FeCl_2$+$FeCl_3$ to β-Fe_2O_3,β-Fe_2O_3 NPs remove methylene blue from water. SEM, UV-Vis, PL, and XRD were used to identify IONPs. Chemically produced β-Fe_2O_3 NPs have an average crystallite size of 10.910730 nm, while Sol-gel-produced NPs are 18.834940 nm. In the simple chemical procedure, the grain size was (4.4 to 205.7) nm and averaged 47.2 nm. In sol-gel, it was (9.1 to 308) nm and averaged 53 nm. Utilizing simple chemicals, the energy gap grew from 1.94 to 3.33 eV, and using sol-gel, it grew from 1.94 to 3.16 eV. Photoluminescence (PL) measurements showed that sol-gel approach created β-Fe_2O_3 nanoparticles had a near band edge emission of 2.75 eV, while the simple chemical process had 2.72 eV. In this experiment, light-exposed NPs broke down MB dye photo catalytically. Sol-gel produces 77.2% degradation at 75 minutes for 3 mg and 88.6% at 150 minutes for 5 mg, while simple chemical produces 43.1% at 75 minutes for 3 mg and 51.7% at 150 minutes for 5 mg.

How to cite this article
Khamees H A., Abid M A. Effects of Different Biosynthesis Methods on the Structural and Optical Properties of Iron Oxide Nanoparticles and Photocatalytic Application. J Nanostruct, 2022; 12(3):999-1012. DOI: 10.22052/JNS.2022.04.021

INTRODUCTION

New nanomaterial developments in the physical, chemical, and biological sciences have gained a lot of interest because of their performance in the production of electronics such as microprocessors, lithium-ion batteries, transistors, emitting diodes, and sensors. In addition to cancer treatments, antimicrobial and antibacterial drugs are derived from them. Among the many vital applications that rely on their use are pollution control catalysts and gas detection systems. When it comes to polluted drinking water, nanomaterials will be able to remove heavy metals as well as organic and inorganic substances [1-6]. Recently, researchers have explored the nanometer-scale structures of metallic oxides in an effort to create ways to monitor those materials. [7]. Just a few examples of metallic oxides include titanium dioxide, zinc oxide, bismuth oxide, copper oxide, and iron oxide (Fe_2O_3)[2, 8]. Iron oxides are widespread natural substances found in both the earth's crust (rocks, bedrock, and water) and living creatures (animals and plants)[9]. Stable Fe_2O_3 NPs are widespread in nature, even at room temperature and pressure. They have a low magnetic field strength [10] and in the majority of cases, do not respond to hand

* *Corresponding Author Email: hussamalshamary77@uomustansiriyah.edu.iq*

magnets [11]. "Green synthesis" is a new area of nanotechnology. Some of the species used in this process include plants, algae, and microbes [12-16]. Iron oxide nanoparticles (IONPs) and other metal oxide nanoparticles can be manufactured in a variety of ways to produce efficient and ecologically friendly metal NPs. Plants can be used in a number of green synthesis techniques for NPs to decrease or remove toxic compounds [10]. NPs of iron oxide (Fe_2O_3) have good environmental and medical uses due to their narrow band gap, chemical stability, and magnetic characteristics [11-14]. Long-term stability is claimed for the ecologically beneficial Fe NP green synthesis. Antimicrobial and cytotoxic characteristics as well as photocatalytic activity in the breakdown of MB dyes, have been demonstrated by Fe NPs. [15]. Shahana B., etal [16] An extract of Cynometra ramiflora fruit is used in the production of IONPs (chemical way). The presence of a dark solution proved the synthesis of IONPs. To show that MB dye had been irradiated for 150 minutes, the absorption peak at 663 nm (a signature of the dye) gradually decreased. Recently, Chauhan etal[17] Lawsonia inermis Conocarpus extract was used to make chemically synthesized iron oxide NPs.. In (2019), Sammy I., etal [17],Preparation IONPs as a catalyst to degrade MB degradation by using Galinsoga parviflora, Conyza bonariensis, and Bidens pilosa extracts using (chemical way). Sol-gel is an example of a bottom-up approach for making NPs. Only a handful of investigations employing the Sol-gel have explored the idea of MB dye breakdown in typical light conditions. The chemical and sol-gel methods of IONP manufacture will be compared in this investigation. Toxic-free, environmentally friendly, and cost-effectively produced NPs with superior crystalline structures can be made with Sol-gel. These NPs have higher purity and are safer for the environment. A major advantage of green synthesis is that it can be easily scaled up for large-scale synthesis and does not require as much energy or hazardous substances as chemical or physical techniques .Green synthesis allows for greater control over crystal growth. Green nanoparticles produced (green NPs) in a factory are cheap and useful [10, 18, 19]. Conocarpus extract and iron (II+III) chloride ($FeCl_2$+$FeCl_3$) were used to make IONPs using simple chemical and sol-gel methods. Drop-casting was used to create these films, which were then characterized in terms of their structural and optical properties. It was decided to employ scanning electron microscopy and high-resolution X-ray diffraction to determine the crystallinity and morphology of the samples produced. UV-VIS spectrophotometers and photoluminescence (PL) measurements were used to investigate these characteristics. Our researchers also examined the disintegration of MB dye under typical lighting conditions.

MATERIALS AND METHODS

$FeCl_2$+$FeCl_3$ (iron (II+III) chloride) and fresh Conocarpus from Baghdad, Iraq, were procured from the local market in Iraq. Vitamins, amino acids, phenolic acid, glycosides, and minerals are all present in this plant. All of the experimental glassware was made with Borosil. Using water, the glass and substrates were sanitized and air-dried at room temperature to remove any contaminants or flaws.

Preparation of the Conocarpus extract

To remove any impurities, the Conocarpus specimens used in this investigation were cleaned, diced, and air dried for 8–10 days. Dried herbs were ground into a fine powder using an industrial

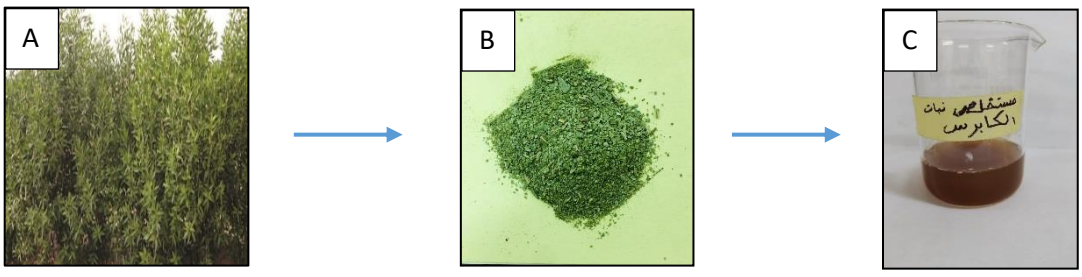

Fig. 1. The method for extracting the conocarpus for 2 hours at 80 degrees Celsius.Conocarpus plant (A), Conocarpus powder (B), Conocarpus extract (C)

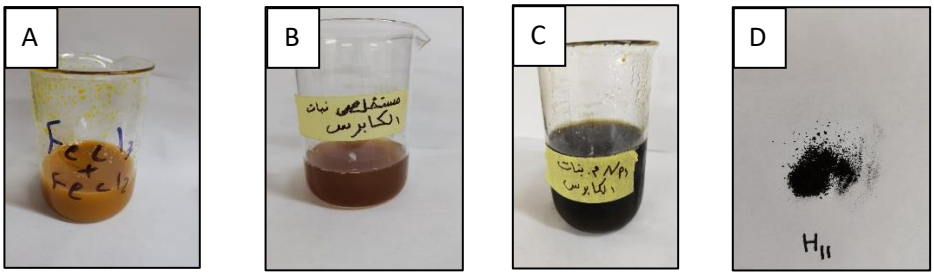

Fig. 2. Stages involved in the transformation of the mixture into IONPs with a simple chemical method include: A) $FeCl_2$ + $FeCl_3$ solution, B) Conocarpus extract, C) β-Fe_2O_3 NPs solution, D) β-Fe_2O_3 NPs powder.

stainless steel blender. The extract was made by dissolving 10g of Conocarpus powder in 100 mL of water. The mixture was heated for two hours at 80 °C using a magnetic stirrer. The final product was ready for use after cooling to room temperature and filtering through Whatman paper.[20]. Fig. 1 depicts the process through which Conocarpus is made into an extract.

Preparation of iron oxide NPs by using Conocarpus extract (By simple chemical)

Conocarpus extract (100 ml) was added to (0.1 M + 0.2 M, 100 mL) of $FeCl_2$+ $FeCl_3$ to produce iron oxide NPs. Then, a magnetic stirrer was used to agitate the solution for 30 minutes at 80 °C. It was immediately apparent that β-Fe_2O_3 NPs had been formed during the manufacture of this substance by the rapid shift in hue from translucent yellow to black. It was then cooled to room temperature. It took two hours at 200 °C to dry out 25 mL of this solution in a ceramic dish in order to produce a fine powder from the solution. IONP solutions were eventually stored in sealed serum tubes for further study. [21]. Fig. 2 demonstrates the usage of iron (II+III) chloride in the preparation of IONPs from Conocarpus extract.

Preparation of IONPs from Conocarpus extract (By sol_gel)

It was done using the sol-gel method, with the addition of 100 mL of Conocarpus extract to $FeCl_2$+$FeCl_3$ (0.1 M+0.2 M,100mL) and constant stirring at 40 °C for one hour and 60 °C for half an hour. Centrifuged at 4000 rpm for 20 minutes, the solution became turbid (cloudy) due to dispersed particles. After the supernatant was collected and dried at 200°C for two hours, the precipitates were filtered. Conocarpus extract with $FeCl_2$ + $FeCl_3$ was used to create IONPs, as shown in Fig. 3 [22].

Characterization of β-Fe_2O_3 NPs Prepared from Conocarpus extract

Analysts used data from the joint committee on powder diffraction standards (JCPDS) card to identify their specimen. Shimadzu's step-by-step examination model (XRD-6000) was used to take XRD measurements across a temperature range of 20°–70°. (Jobin-Yvon HR800UV) employed a double-beam spectrophotometer to examine the power spectrum.

P*hotocatalytic activity of iron oxide NPs by using Conocarpus extract under normal light*

A known amount of MB dye solution (1 mg, 3×10^{-5} M) was combined with 100 mL of deionized water to make a final MB dye solution concentration

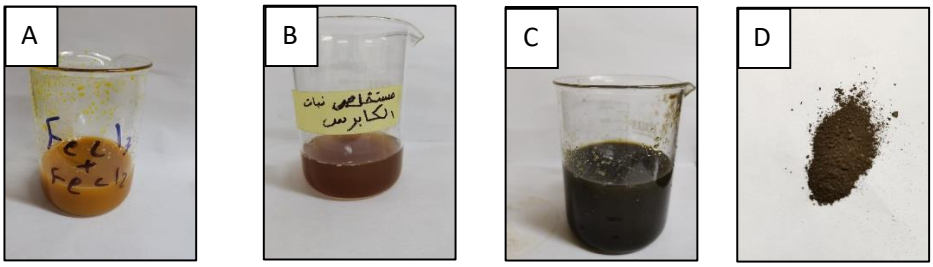

Fig. 3. Steps converting the mixture into iron oxide NPs with the sol-gel method, A) $FeCl_2$ + $FeCl_3$ solution, B) Conocarpus extract, C) β-Fe_2O_3 NPs solution, D) β-Fe_2O_3 NPs powder.

of 10 mg/L to test the photocatalytic activity of the IONPs. When 3 mg of iron oxide NP powder was added for the first time, the suspension was swirled for 5 minutes in total darkness using a magnetic stirring device to maintain equilibrium. After 5 minutes, the combination was subjected to a direct normal (115 mW/mm^2 intensity, as measured by SM206 solar power meter). It is 0.15 meters from the source of light. In the end, 5 mL of the suspension was centrifuged for 20 minutes at 4000 rpm, and the absorbance was measured using a Shimadzu UV-1800 spectrophotometer. The greatest absorption rate may be observed at a wavelength of 664 nm. Dye molecular interactions with adsorbed substances are principally influenced by surface modifications on both the dye molecular and the adsorbent material [23]. the experiment was repeated at 5 mg every 10 minutes.

The degradation efficiency of MB dye was calculated using the following equation :

According to this method, the MB dye degradation percentage was determined by Eq.

$$\text{Degradation percentage } (\%) = [\,1 - \frac{\text{Cfin}}{\text{Cini}}\,] \times 100\ \%$$

Where: Cini = the original (MB) dye concentration, Cfin = the dye concentration at the end.

The kinetic constant rate (Kph) of the MB dye degradation was calculated using Eq. (2):

$$\ln[\,Cini/Cfin] = Kph \times t$$

Where: Cini = the original (MB) dye concentration, Cfin= the dye concentration at the end,

Kph= constant rate of MB dye, t = radiation time.

The MB dye degradation efficiency can be calculated using the following equation:

$$\text{Efficacy of degradation } (\%) = [\,\text{Cini} - \frac{\text{Cfin}}{\text{Cini}}\,] \times 100\ \%$$

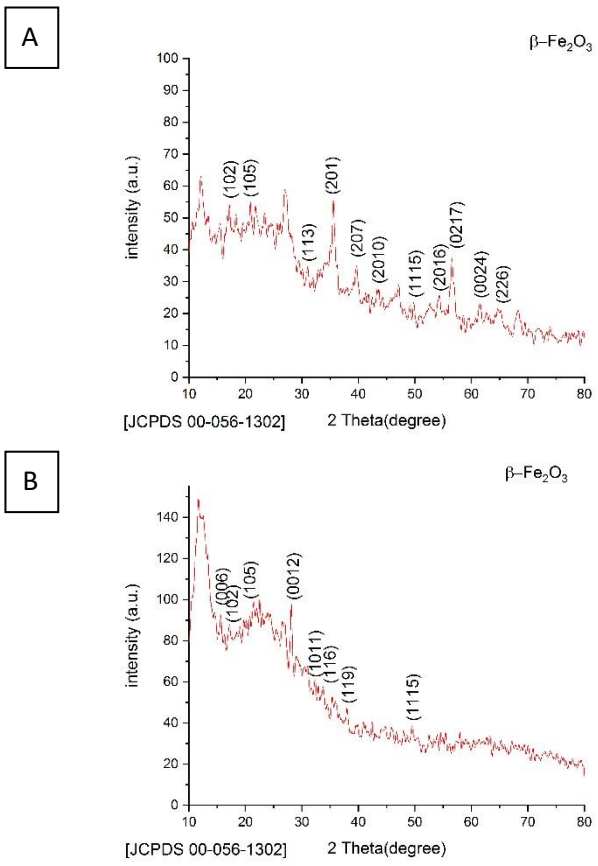

Fig. 4. XRD pattern of IONPs extracted from Conocarpus using $FeCl_2$+ $FeCl_3$ salt for 2 hours at 200 °C (A) simple chemical, (B) sol-gel method.

Table 1. XRD results for β-Fe_2O_3 NPs from Conocarpus extract using $FeCl_2$+$FeCl_3$ salt for 2h, 200 °C with simple chemical and sol-gel method.

Method	Plant extract	Material	FWHM (deg.)	Plane (hkl)	Crystallite size D (nm)
Simple chemical	Conocarpus	β-Fe_2O_3	0.75	201	11.06972
			0.7	207	12.83431
			0.9	0217	8.828182
Sol-gel	Conocarpus	β-Fe_2O_3	2.4	006	3.310491
			0.2	102	39.65497
			0.6	0012	13.53936

Where: Cini = the original (MB) dye concentration, Cfin = the dye concentration at the end.

RESULTS AND DISCUSSION

Synthesis and characterization of iron oxide NPs by using Conocarpus extract

Reaction conditions in the modern plant include a mixture of Conocarpus extract and iron extract. Nanoparticle generation, field, and stability can be controlled by the Conocarpus extract's parameters. The phytochemicals in Conocarpus extract can lower the quantity of iron that has been used up in a short period of time. Conocarpus extract also has a key role in lowering and stabilizing a number of parameters in the

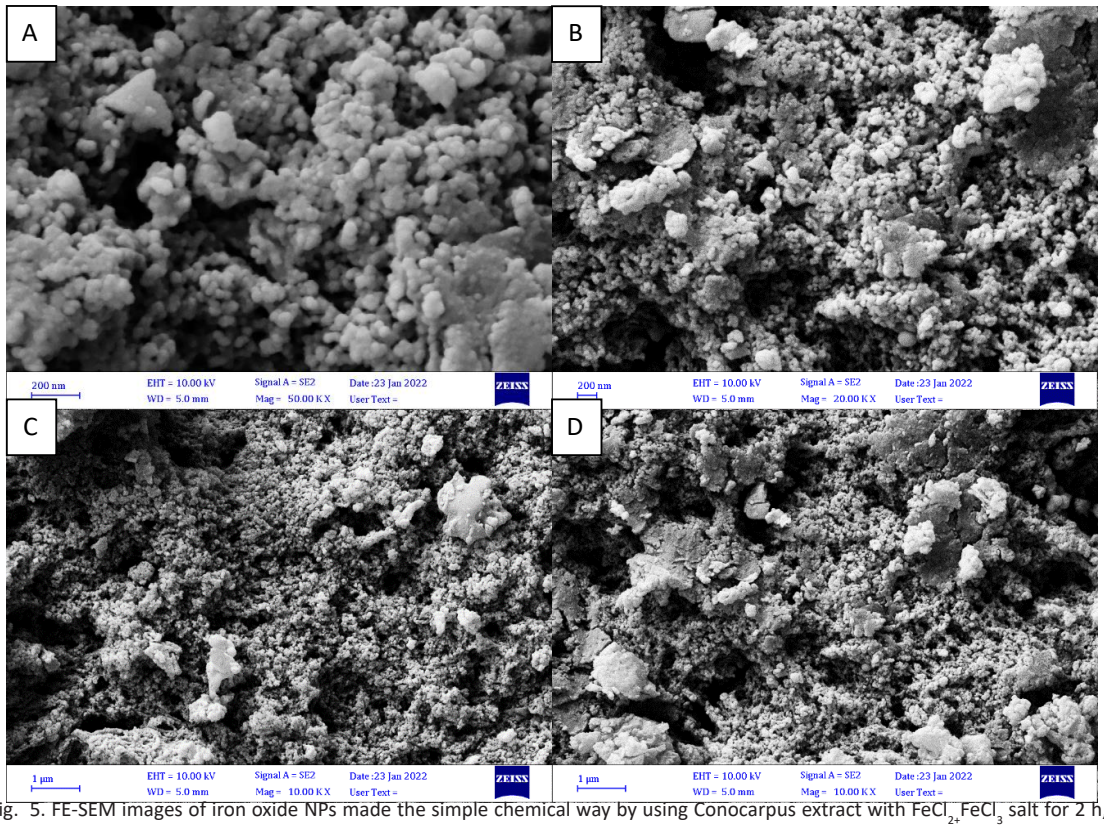

Fig. 5. FE-SEM images of iron oxide NPs made the simple chemical way by using Conocarpus extract with $FeCl_{2+}FeCl_3$ salt for 2 h, 200 °C.

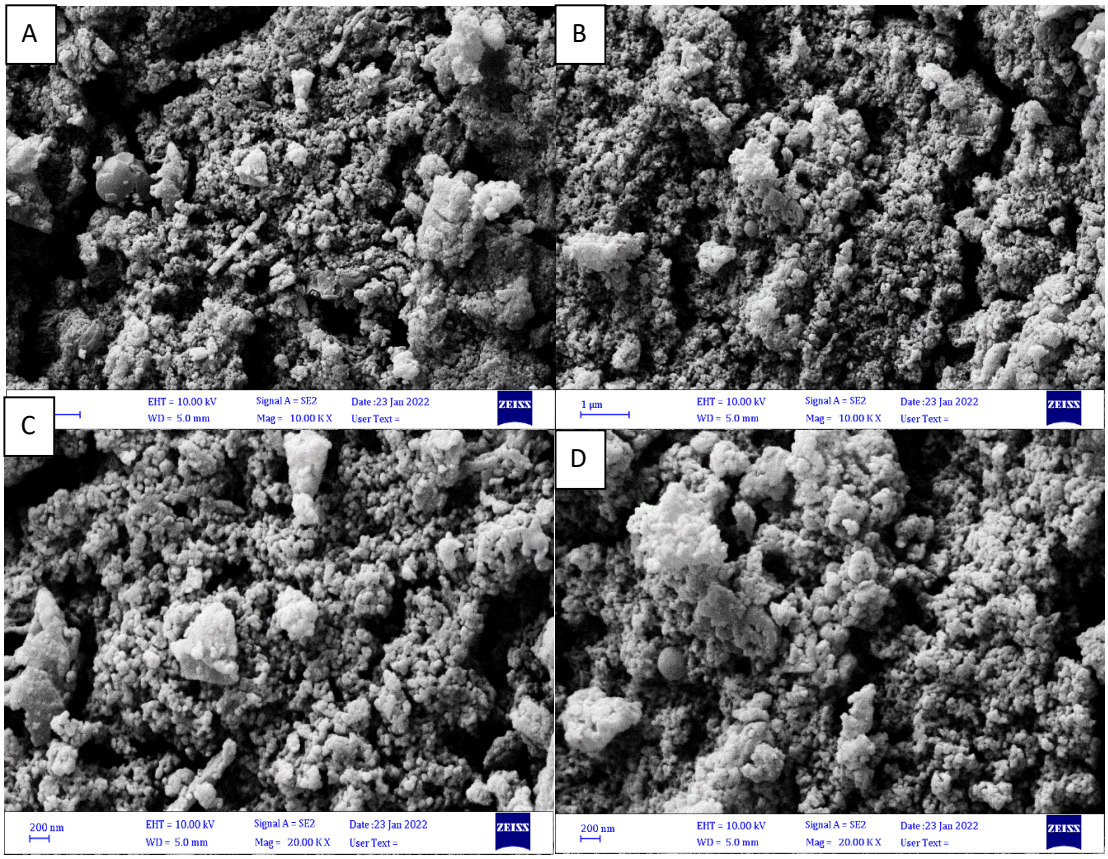

Fig. 6. FE-SEM images of iron oxide NPs made sol-gel way by using Conocarpus extract with $FeCl_2$+$FeCl_3$ salt for 2 h, 200 °C.

simple manufacture of iron oxide NPs.

The XRD analysis of iron oxide NPs (β-Fe_2O_3) prepared by using Conocarpus extract with iron

It is possible to determine the material, structure, and orientation of materials using XRD analysis in this research. $FeCl_2$+$FeCl_3$ were dissolved in Conocarpus extract for 2 hours at 200 °C. The IONPs were made by utilizing a simple chemical and Sol-gel process, and the results were impressive. In a simple chemical method, the peaks of the crystalline (β-Fe_2O_3) phase (wustite, space group Fm-3m, JCPDS no. (00-056-1302)) is

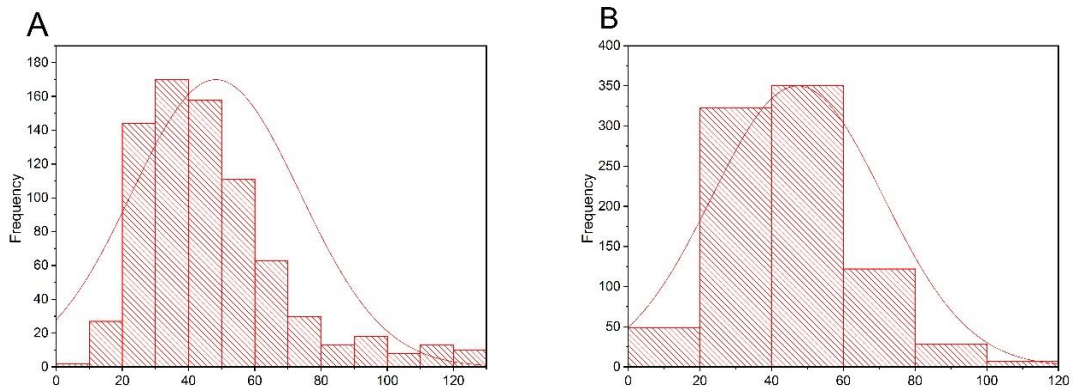

Fig. 7. Particle size distribution A) sol-gel way B)simple chemical way

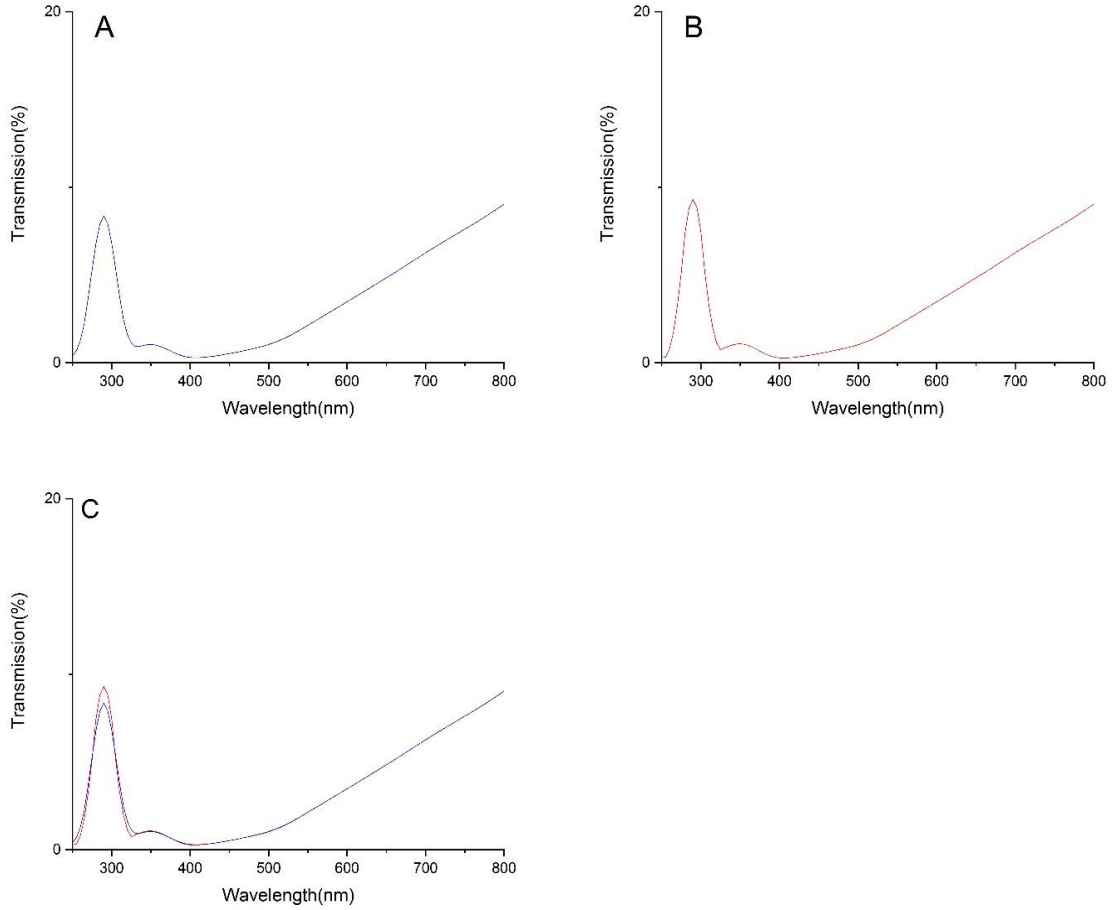

Fig. 8. UV–VIS transmission spectra of iron oxide NPs prepared by using Conocarpus extract in $FeCl_2$+$FeCl_3$ salt for 2 hours at 200 °C using sol-gel and a simple chemical method (A).sol-gel (B). A simple chemical (C) Both sol-gel and simple chemicals.

(102) corresponding to (105),(113),(201),(207),(2 010),(1115),(2016),(0217),(0024),and(226) millers indices and in sol-gel method (JCPDS no. (00-056-1302)) is (006) corresponding to (102),(105),(0012),(1011),(116),(119)and(1115) millers indices , as shown in Fig. 4[24, 25]. The results of IONPs (β - Fe_2O_3) phases, and crystallite size appear in table (1). The crystallite size (D) was determined. applied the following: Scherrer's formula [26, 27].

$$D\ (nm) = \frac{k.\lambda}{\beta\cos\theta}$$

Where: λ is wavelength (0.15418) nm (CuK_α), k is shape factor (0.9), β is full width at half maximum (FWHM) and θ is diffraction angle[27].

The FE-SEM images of IONPs (β-Fe_2O_3) prepared from Conocarpus extract by $FeCl_2$+$FeCl_3$ extract

An FE-SEM imaging technique was employed at a temperature of 200 °C to examine the distribution of size and surface morphology of IONPs produced from Conocarpus extract and iron (II+III) chloride. Fig. 5 (A-B-C-D) shows the morphology of β-Fe_2O_3 NPs (wustite) in the chemical process, where the grain size ranges from 4.4 nm to 205.7 nm, average grain size 47.2 nm and the morphology is (nanoparticles-like structure) [28]. And For β-Fe_2O_3 (wustite) NPs, the grain size ranges from 9.1 nm to 308 nm, average grain size 53 nm in the sol-gel process, and the morphology is a (Nano-assemblies due to high thermal energy) structure,

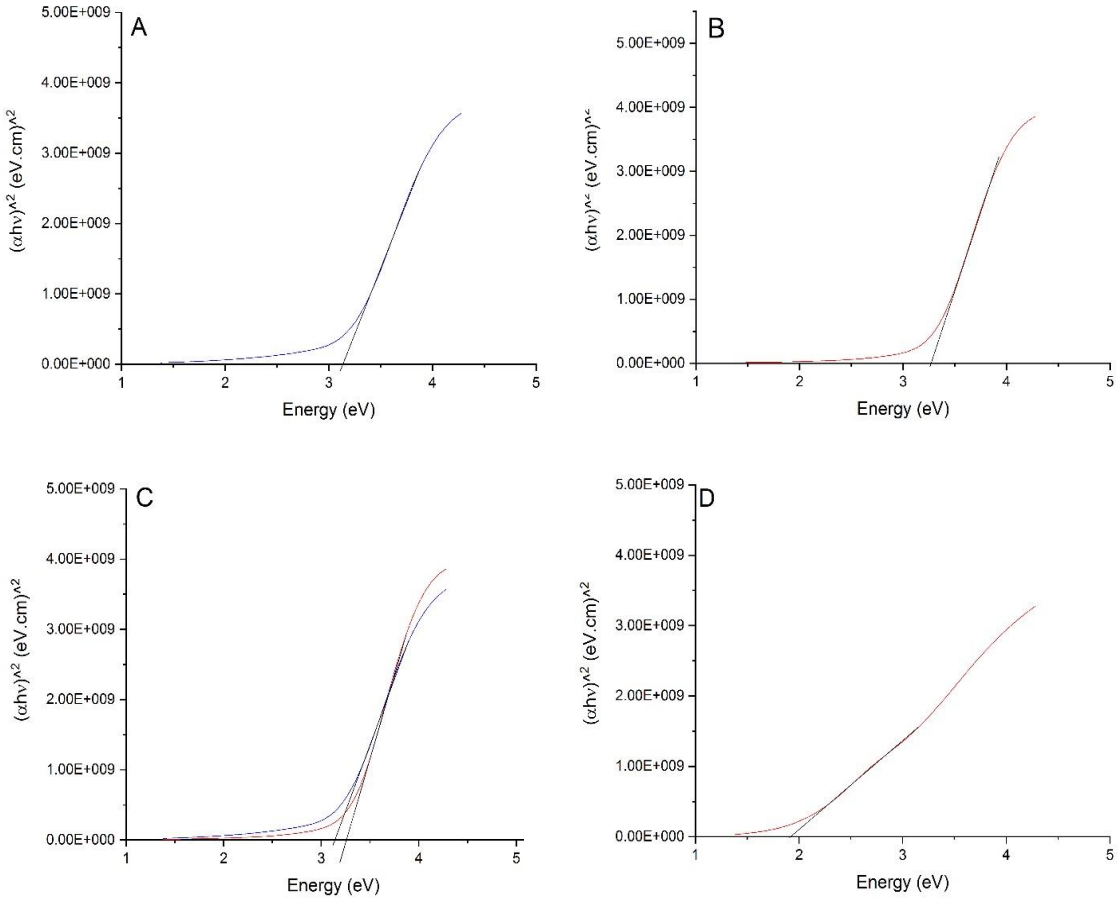

Fig. 9. Energy band gap of iron oxide NPs prepared from Conocarpus extracted by $FeCl_2$+$FeCl_3$ salt A) sol-gel way B) simple chemical way C) Both sol-gel and simple chemical way for 2 h, 200 °C D)bulk$FeCl_2$+$FeCl_3$ material.

as shown in Fig. 6. (A-B-C-D) [29]. The difference in the amount of biomaterial between the extracts and the difference in the reaction mechanism of the two methods led to the appearance of different images in the FESEM examination of iron oxide NPs and the particle size range.

UV–Vis Spectrophotometer of Iron oxide NPs by sol-gel and simple chemical

As shown in Fig. 7, (A-B-C), conocarpus extract mixed with $FeCl_2$ and $FeCl_3$ salt is used to determine the optical transmittance spectra of Fe_2O_3 nanoparticles. [30] . Fig. 8 (A-B-C) appears the energy band gap for β-Fe_2O_3 NPs prepared by a sol-gel and simple chemical way by Conocarpus extract, estimated by plotting the square of $(\alpha h\upsilon)^2$ vs the photon energy (hυ) with sol-gel and simple chemical methods. Using a straight line extrapolation to $(\alpha h\upsilon)^2$, the energy band gap can be calculated. Because of the small size of NPs that reduce the potential attraction between the conduction electrons and metal ions of the particle that leads to the band energy gap increases for the smaller particles, or may be the concentration increase leads to the division of the level into secondary levels that called energy gap [31, 32]. According to the arrangement and distribution of atoms in the crystal lattice of a powder crystal, the energy band gap can vary in a variety of different ways. The values of the optical band gap for β-Fe_2O_3 NPs ranged from 1.94 to 3.16 eV in the sol-gel method Fig. 8 (A-C)[31]. The optical band gaps of β-Fe_2O_3 NPs measured by the simple chemical technique ranged from 1.94 to 3.3 eV. Fig. 8 (B-C) [32]. The energy band gap can be calculated by using the equation below [9, 33].

$$(\alpha h\upsilon)^n = A\,(h\upsilon - Eg)$$

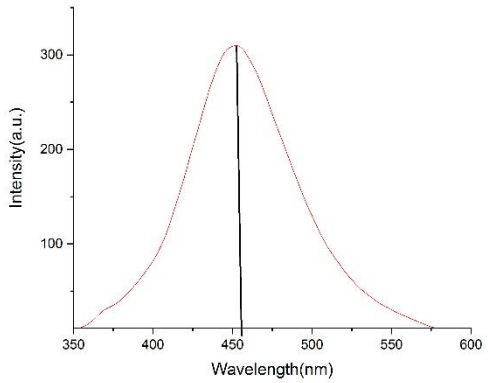

Fig. 10. The PL spectra of iron oxide NPs as-prepared by using Conocarpus extract with $FeCl_2$+$FeCl_3$ salt with a simple chemical method for 2 h, 200 °C.

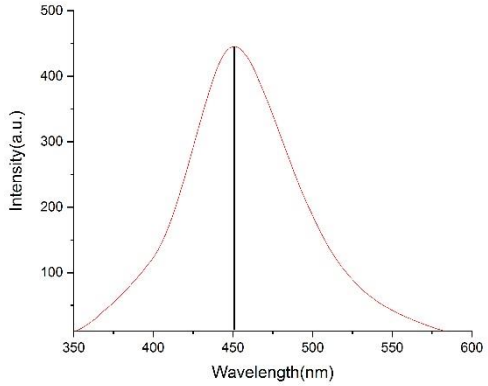

Fig. 11. The PL spectra of iron oxide NPs as-prepared by using Conocarpus extract with $FeCl_2$+$FeCl_3$ salt by the sol-gel method for 2 h, 200 °C.

Fig. 12. The images of the steps of the degradation of the MB dye in 1) original dye, 2) in darkness by β-Fe_2O_3 (IONPs) , 3) after 5 min, 4) after 10 min, and 5) after 15 min 6) after 20 min, 7) after 25 min, until 75 min, by Sol-gel (A) and simple chemical (B) techniques.

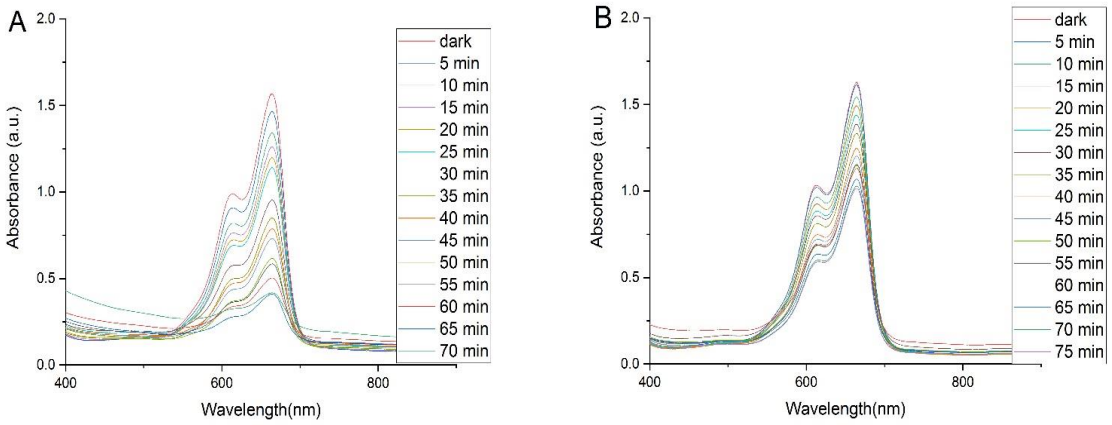

Fig. . 13. The degradation image for the MB dye with iron oxide NPs, A) Sol-gel method, B) Chemical method ,with normal light from Conocarpus extracted by $FeCl_{2+}$ $FeCl_3$ salt for 2 h,200 °C .

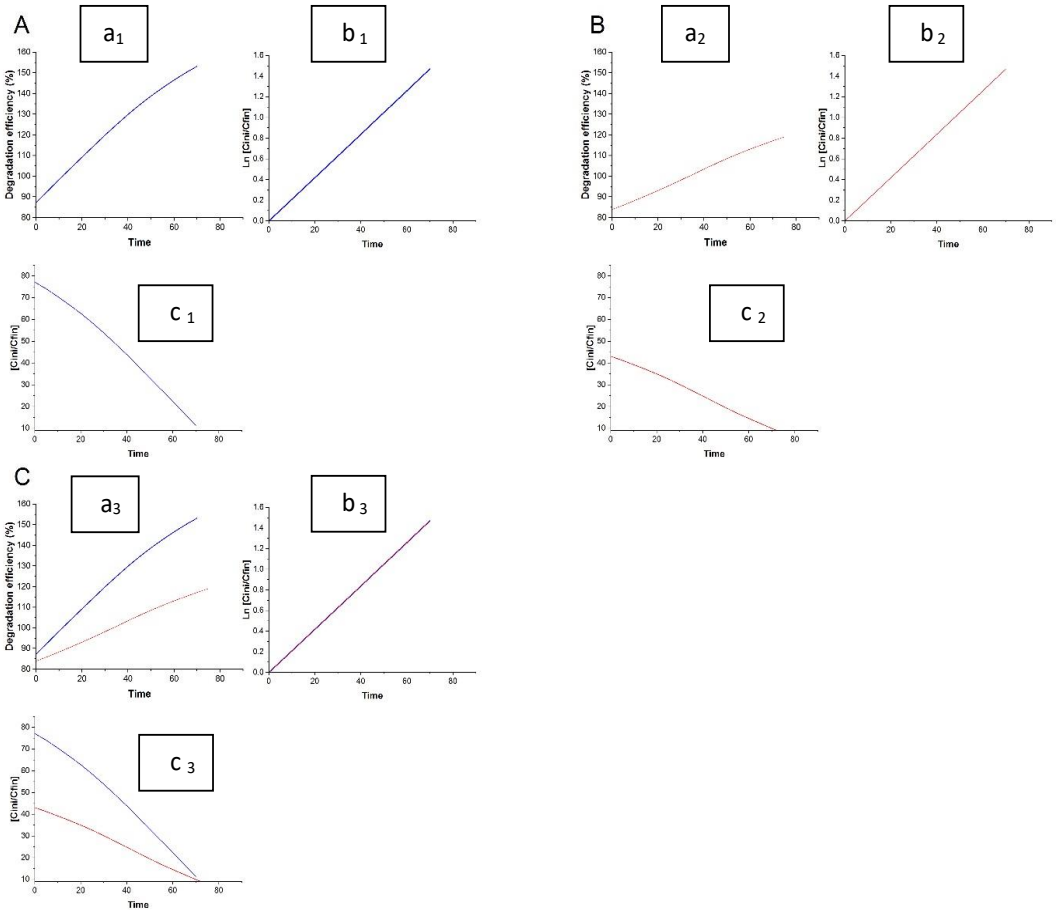

Fig. 14. (a) The degradation efficiency (%) of MB dye at 10 mg/L by iron oxide NPs prepared from Conocarpus extract with $FeCl_{2+}$ $FeCl_3$ salt for 2 h, 200 °C. (b) In the presence of iron oxide NPs, the degradation of MB dye is plotted as a linear function of light intensity in the same conditions, (c) The percentage of MB dye degradation. A) Sol-gel method, B) Simple chemical method and C) Both sol-gel and simple chemical methods respectively.

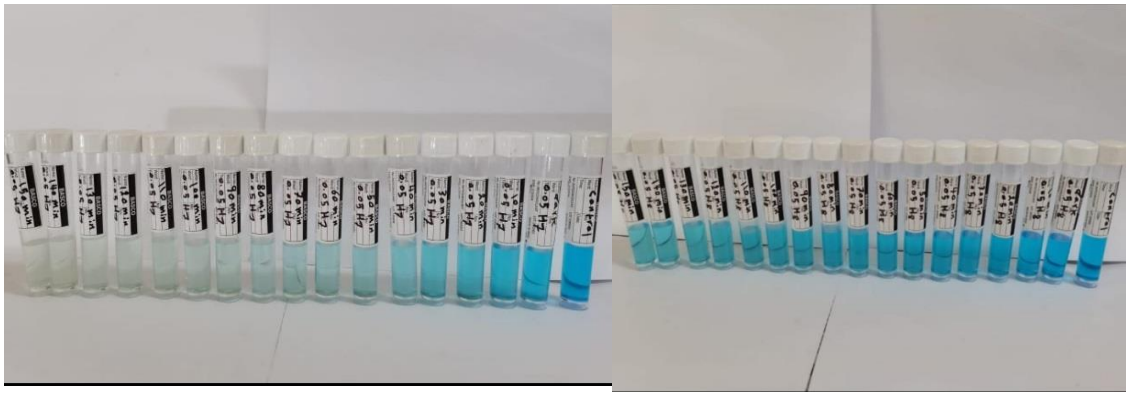

Fig. 15. The images of the steps of the degradation of the MB dye in 1) original dye, 2) in the dark by $FeCl_2$+$FeCl_3$, 3) after 10 min, 4) after 20 min, 5) after 30 min, 6) after 40 min, 7) after 50 min, until 150 min , by Sol-gel (A) and simple chemical (B)

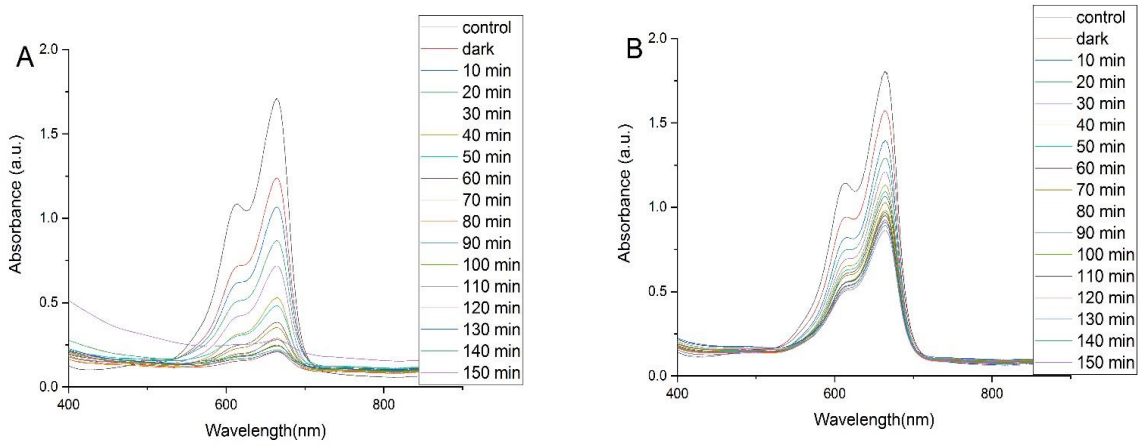

Fig. 16. The degradation of MB dye with iron oxide NPs, A) in the sol-gel method, B) in the chemical method, with normal light by using Conocarpus extract with $FeCl_2$+ $FeCl_3$ salt for 2 h, 200 °C.

Where :A is constant, hυ is the energy of light, and, α is the absorption coefficient, n: is a constant depending on the nature of the electron transition [33]. In comparing the iron oxide NPs prepared with a sol-gel and a simple chemical method from Conocarpus extracted by $FeCl_2$ +$FeCl_3$ salt,the energy band gap showed a distinct blue shift, from 1.94 eV to 3.16 and 3.3eV respectively for β-Fe_2O_3 NPs. The decrease in the crystal size and the particle size causes an increase in the optical band gap according to the principle of quantum confinement.

The PL spectrum of iron oxideNPs (β-Fe_2O_3) prepared by using Conocarpus extract with $FeCl_2$+$FeCl_3$ extract

At the near-band edge of the PL spectrum, iron oxide NPs synthesized by simple chemical and sol-gel procedures from Conocarpus extract with $FeCl_2$+$FeCl_3$ at (200 ◦C) can be seen. As shown in Fig. 9, the excitation band of β-Fe2O3 NPs at 200 ◦C has an excitation wavelength of 325 nm (wustite, the near wavelength (455.56 nm), which is the near-band edge of (2.72) eV. Fig. 10 shows that the near band edge of β-Fe_2O_3 NPs (wustite, the near wavelength (450.83 nm) at 200 ◦C in the sol-gel process is (2.75) eV with the exaction band being 325 nm.

The difference in the type of extract, the amount of biomaterial it contains, and the method of preparing the nanomaterial had an effect on the value of the near band edge.

Photocatalytic activity of iron oxide NPs from Conocarpus extract under normal light

The photocatalytic reaction follows the

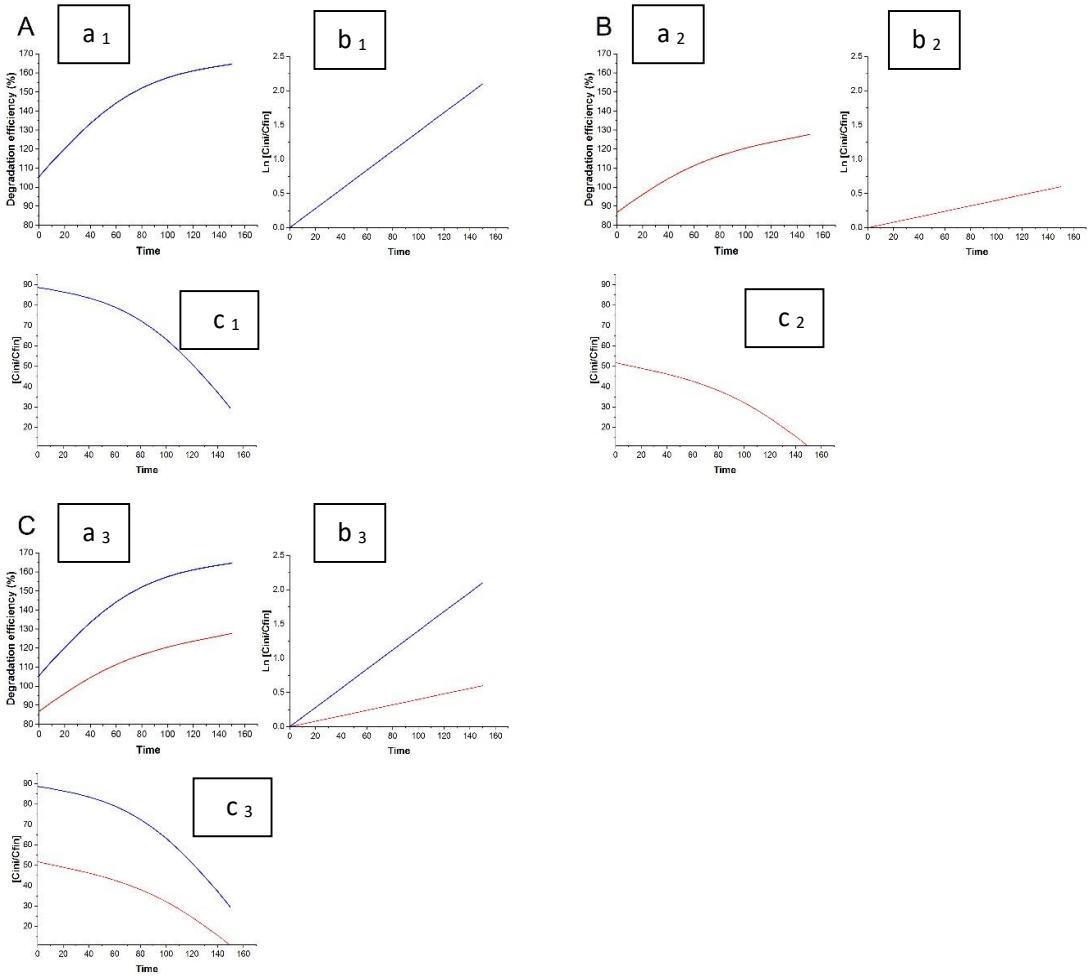

Fig. 17. (a) Degradation efficiency (%) of MB dye at 10 mg/L by iron oxide NPs prepared by using Conocarpus extract in $FeCl_2$+ $FeCl_3$ salt for 2 h, 200 °C.(b) Linear plot of degradation of MB dye under normal light irradiation in the presence of iron oxide NPs in the same conditions. (c) The percentage degradation of MB dye, A) Sol-gel method, B) Simple chemical method and C) Both sol-gel and simple chemical methods, respectively.

following basic mechanism: when β-Fe2O3 NPs are exposed to normal light at room temperature, electron-hole pairs are generated, as shown in Eq.1, electrons can be excited from the valance band to the conduction band, and holes are formed in the valance band. These holes and electrons interact with H2O and O2 in the extract solution, respectively, as shown in Eq. 2 and Eq. 3 to yield the OH and OOH hydroxyl radicals, as shown in Eq. 4. These hydroxyl radicals, which are highly oxidizing in nature, can completely oxidize the dyes by abstracting electrons from dye molecules and by breaking the large organic materials into less harmful small organic materials, as shown in Eq. 5 [9].

$$IONPs + h\nu \rightarrow e^- + h^+ \quad (1)$$

$$e^- + O_2 \rightarrow \cdot O^{2-} \quad (2)$$

$$h^+ + H_2O/OH^- \rightarrow \cdot OH \quad (3)$$

$$O^{2-} + H_2O \rightarrow \cdot OOH + OH^- \quad (4)$$

$$OH + MB \rightarrow CO_2 + H_2O \quad (5)$$

From the above Photocatalytic activity patterns, it is noticed that the maximum Photocatalytic activity by IONPs with 5 mg is corresponding to the sol-gel method with using Conocarpus extracts because of a high surface area and aspect ratio.

CONCLUSION

Chemical and sol-gel methods were used to synthesize IONPs (β-Fe_2O_3) from the Conocarpus extract and $FeCl_2$+$FeCl_3$ without the need for any catalytic chemical material. It was found that the crystalline size of β-Fe_2O_3 NPs with a chemical technique was approximately 10.910730 nm, whereas the crystalline size of NPs with the Sol-gel method was about 18.834940 nm at 200 ◦C using Conocarpus extract. For β-Fe_2O_3 NPs (wustite), the average grain size measured by FESEM at 200 ◦C using Conocarpus extract ranged from 4.4 nm to 205.7 nm and average grain size 47.2 nm in chemical way and from 9.1 nm to 308 nm and average grain size 53 nm in sol-gel way. Using Conocarpus as a PL spectrum, the optical near band edge value was shifted to the blue by (2.72) eV in chemical and (2.75) eV in sol-gel. Iron oxide nanoparticles (NPs) were found to have photocatalytic activity in environmental treatments. According to the results, the synthesized material is of high quality β-Fe_2O_3 NPs, with greater degradation efficiency when made using the sol-gel technique, reaching 77.2% at 75 minutes for 3 mg and 88.6% at 150 minutes for 5 mg, with a higher level of photocatalytic efficacy than the β-Fe_2O_3 with a simple chemical method, whereas degradation efficiency was 43.1% at 75 minutes for 3 mg and 51.7 percent at 150 minutes for 5 mg.

CONFLICT OF INTEREST

The authors declare that there is no conflict of interests regarding the publication of this manuscript.

REFERENCES

1. Ali A, Zafar H, Zia M, ul Haq I, Phull AR, Ali JS, et al. Synthesis, characterization, applications, and challenges of iron oxide nanoparticles. Nanotechnology, Science and Applications. 2016;Volume 9:49-67.
2. Villesque-Dubus F, Mannarini M, Rouissi M. Chapitre 2. Systme de contrle et systme de gestion: le cas du changement numrique dans une banque. Comptabilits et Socit: EMS Editions; 2018. p. 67.
3. Schrier L, Hadjipanayis A, Stiris T, Ross-Russell RI, Valiulis A, Turner MA, et al. Off-label use of medicines in neonates, infants, children, and adolescents: a joint policy statement by the European Academy of Paediatrics and the European society for Developmental Perinatal and Pediatric Pharmacology. Eur J Pediatr. 2020;179(5):839-847.
4. Dinesh D, Murugan K, Madhiyazhagan P, Panneerselvam C, Mahesh Kumar P, Nicoletti M, et al. Mosquitocidal and antibacterial activity of green-synthesized silver nanoparticles from Aloe vera extracts: towards an effective tool against the malaria vector Anopheles stephensi? Parasitol Res. 2015;114(4):1519-1529.
5. Jawed A, Saxena V, Pandey LM. Engineered nanomaterials and their surface functionalization for the removal of heavy metals: A review. Journal of Water Process Engineering. 2020;33:101009.
6. Jawed A, Pandey LM. Application of bimetallic Al-doped ZnO nano-assembly for heavy metal removal and decontamination of wastewater. Water Sci Technol. 2019;80(11):2067-2078.
7. Hameed SA. Effect of Thickness on Structural and Optical Properties of CdO Thin Films Prepared by Chemical Spray Pyrolysis Method. Neuroquantology. 2020;18(4):20-26.
8. Paul E, Ramis J-P. Dynamics on Wild Character Varieties. Symmetry, Integrability and Geometry: Methods and Applications. 2015.
9. Abid MA, Kadhim DA. Novel comparison of iron oxide nanoparticle preparation by mixing iron chloride with henna leaf extract with and without applied pulsed laser ablation for methylene blue degradation. Journal of Environmental Chemical Engineering. 2020;8(5):104138.
10. Klaus-Joerger T, Joerger R, Olsson E, Granqvist C-G. Bacteria as workers in the living factory: metal-accumulating bacteria and their potential for materials science. Trends Biotechnol. 2001;19(1):15-20.
11. Zhao M, Li M, Liu RJ. Effects of arbuscular mycorrhizae on microbial population and enzyme activity in replant soil used for watermelon production. International Journal of Engineering, Science and Technology. 2011;2(7).
12. Muthukumar H, Gire A, Kumari M, Manickam M. Biogenic synthesis of nano-biomaterial for toxic naphthalene photocatalytic degradation optimization and kinetics studies. International Biodeterioration & Biodegradation. 2017;119:587-594.
13. Sharma S, Hasan A, Kumar N, Pandey LM. Removal of methylene blue dye from aqueous solution using immobilized Agrobacterium fabrum biomass along with iron oxide nanoparticles as biosorbent. Environmental Science and Pollution Research. 2018;25(22):21605-21615.
14. Tiwari S, Hasan A, Pandey LM. A novel bio-sorbent comprising encapsulated Agrobacterium fabrum (SLAJ731) and iron oxide nanoparticles for removal of crude oil co-contaminant, lead Pb(II). Journal of Environmental Chemical Engineering. 2017;5(1):442-452.
15. Alshehri A, Malik MA, Khan Z, Al-Thabaiti SA, Hasan N. Biofabrication of Fe nanoparticles in aqueous extract of Hibiscus sabdariffa with enhanced photocatalytic activities. RSC Advances. 2017;7(40):25149-25159.
16. Bishnoi S, Kumar A, Selvaraj R. Facile synthesis of magnetic iron oxide nanoparticles using inedible Cynometra ramiflora fruit extract waste and their photocatalytic degradation of methylene blue dye. Materials Research Bulletin. 2018;97:121-127.
17. Wanakai SI, Kareru PG, Makhanu DS, Madivoli ES, Maina EG, Nyabola AO. Catalytic degradation of methylene blue by iron nanoparticles synthesized using Galinsoga parviflora, Conyza bonariensis and Bidens pilosa leaf extracts. SN Applied Sciences. 2019;1(10).
18. Namvar F, Mohammad R, Baharara J, Mahdavi M, Amini E, Yeap SK, et al. Cytotoxic effect of magnetic iron oxide nanoparticles synthesized via seaweed aqueous extract. International Journal of Nanomedicine. 2014:2479.
19. Allouche J. Synthesis of Organic and Bioorganic Nanoparticles: An Overview of the Preparation Methods. Nanomaterials: A Danger or a Promise?: Springer London;

2012. p. 27-74.
20. Ns AK, S A, Malingappa P. Nano zinc ferrite modified electrode as a novel electrochemical sensing platform in simultaneous measurement of trace level lead and cadmium. Journal of Environmental Chemical Engineering. 2018;6(6):6939-6946.
21. Beheshtkhoo N, Kouhbanani MAJ, Savardashtaki A, Amani AM, Taghizadeh S. Green synthesis of iron oxide nanoparticles by aqueous leaf extract of Daphne mezereum as a novel dye removing material. Appl Phys A. 2018;124(5).
22. Perveen R, Shujaat S, Qureshi Z, Nawaz S, Khan MI, Iqbal M. Green versus sol-gel synthesis of ZnO nanoparticles and antimicrobial activity evaluation against panel of pathogens. Journal of Materials Research and Technology. 2020;9(4):7817-7827.
23. Maurya NS, Mittal AK, Cornel P, Rother E. Biosorption of dyes using dead macro fungi: Effect of dye structure, ionic strength and pH. Bioresour Technol. 2006;97(3):512-521.
24. Zhang N, Guo Y, Wang X, Zhang S, Li Z, Zou Z. A beta-Fe_2O_3 nanoparticle-assembled film for photoelectrochemical water splitting. DTr. 2017;46(32):10673-10677.
25. Malina O, Kaslik J, Tucek J, Cuda J, Medrik I, Zboril R. Thermally-induced solid state transformation of Fe_2O_3 nanoparticles in various atmospheres. AIP Conf Proc: AIP Publishing LLC; 2014.
26. Shipley HJ, Engates KE, Guettner AM. Study of iron oxide nanoparticles in soil for remediation of arsenic. Journal of Nanoparticle Research. 2010;13(6):2387-2397.
27. Kianpour S, Ebrahiminezhad A, Mohkam M, Tamaddon AM, Dehshahri A, Heidari R, et al. Physicochemical and biological characteristics of the nanostructured polysaccharide-iron hydrogel produced by microorganism Klebsiella oxytoca. J Basic Microbiol. 2016;57(2):132-140.
28. A. Ismail A. A Facile Synthesis of α-Fe_2O_3/Carbon Nanotubes and Their Photocatalytic and Electrochemical Sensing Performances. International Journal of Electrochemical Science. 2019:15-32.
29. Barathi P, Devaraj A, Subramania A. Mesoporous Carbon/α-Fe_2O_3 Nanoleaf Composites for Disposable Nitrite Sensors and Energy Storage Applications. ACS Omega. 2020;5(50):32160-32170.
30. Sandhya J, Kalaiselvam S. Biogenic synthesis of magnetic iron oxide nanoparticles using inedible borassus flabellifer seed coat: characterization, antimicrobial, antioxidant activity and in vitro cytotoxicity analysis. Materials Research Express. 2020;7(1):015045.
31. Badawi A, Ahmed EM, Mostafa NY, Abdel-Wahab F, Alomairy SE. Enhancement of the optical and mechanical properties of chitosan using Fe_2O_3 nanoparticles. Journal of Materials Science: Materials in Electronics. 2017;28(15):10877-10884.
32. Bouhjar F, Ullah S, Chourou ML, Mollar M, Marí B, Bessaïs B. Electrochemical Fabrication and Characterization of p-CuSCN/n-Fe_2O_3 Heterojunction Devices for Hydrogen Production. Journal of The Electrochemical Society. 2017;164(13):H936-H945.
33. Soltan WB, Nasri S, Lassoued MS, Ammar S. Structural, optical properties, impedance spectroscopy studies and electrical conductivity of SnO_2 nanoparticles prepared by polyol method. Journal of Materials Science: Materials in Electronics. 2017;28(9):6649-6656.